TECHNICAL MEMORANDUM

416

Singular vector–based multivariate normal sampling in ensemble prediction

M. Ehrendorfer[1] and A. Beck[2]

Research Department

[1]Institute for Meteorology and Geophysics, University of Innsbruck
[2]Department of Meteorology and Geophysics, University of Vienna

August 2003

European Centre for Medium-Range Weather Forecasts
Europäisches Zentrum für mittelfristige Wettervorhersage
Centre européen pour les prévisions météorologiques à moyen terme

For additional copies please contact

The Library
ECMWF
Shinfield Park
Reading
RG2 9AX
library@ecmwf.int

Series: ECMWF Technical Memoranda

A full list of ECMWF Publications can be found on our web site under:
http://www.ecmwf.int/publications/

1 Introduction

Transient growth in atmospheric dynamics has been studied extensively through singular vectors (SVs) that describe perturbations amplifying most rapidly over a finite time for a specified norm (Buizza and Palmer 1995). These SVs allow for an extension of stability analysis beyond structure–preserving normal modes (Farrell and Ioannou 1996). In addition, due to identifying highly sensitive directions in phase space, SVs are primary candidates for generating perturbed initial conditions within ensemble prediction (Molteni et al. 1996).

In the work described in this Technical Memorandum the properties of ensembles that are created through randomly sampling from a multinormal probability density, the covariance structure of which is described by SVs. It is discussed (see, section 2) that SVs computed using analysis–error covariance information provide a square–root decomposition of the analysis error covariance matrix P^{a}. This *SV–decomposition* (see section 2) evolves into the *eigendecomposition* of the forecast error covariance matrix P^{f}. As such, the SV–decomposition of P^{a} is a primary candidate for generating – from a multivariately standard–normal random variable – a set of M initial–time perturbations fully consistent with P^{a} as described through the leading N SVs. Within the Special Project SPATME01 entitled *SV–based multivariate normal sampling in ensemble prediction* this SV–based multinormal sampling technique has been tested with the aim of assessing its potential for operational implementation (especially in the case $M > N$). Specifically, ensembles using SVs based on the total–energy norm have been investigated with this sampling technique (see sections 3 and 4), which has been incorporated into the ECMWF Integrated Forecast System. Another important part of this Special Project is formed by data assimilation and ensemble prediction experiments with an exact quasigeostrophic Kalman Filter which allows for assessing explicitly the implications of limiting initial–time covariance information to N SVs on the time–evolving covariance structures (see section 5).

This Technical Memorandum is based on the final report for the Special Project SPATME01 that lasted from 1 January 2000 to 31 December 2003. Three persons have been working on the project: A. Beck, M. Ehrendorfer (Principal Investigator), and P. Haas. An important achievement during the project was the implementation of the sampling technique (see section 2) within the ECMWF Integrated Forecast System in 2000 (see also section 6 and appendix A). The work and various visits during this Special Project were also strongly connected to Project P13729–GEO funded by the Austrian Science Foundation (see, Ehrendorfer et al. 2003).

2 The SV–based multinormal sampling method

The basic idea of the multinormal sampling consists of generating perturbations consistent with the analysis error covariance matrix, represented through SVs. Theoretical aspects are discussed in Ehrendorfer (1999b), and briefly revisited here. The multinormal sampling by construction generates a set of independent perturbations that is fully consistent with knowledge about the analysis error covariance P^{a} as described through the SVs; the sampling method also ensures that these perturbations are comparable in magnitude to the prespecified amplitude of the operationally used rotation method (Molteni et al. 1996).

2.1 Uncertainty prediction: Hessian SVs

The Hessian SVs (HSVs) are defined as the structures Z_0 that solve the eigenvector problem:

$$\mathsf{M}^{\mathrm{T}}\mathsf{C}^{\mathrm{T}}\mathsf{C}\mathsf{M}\mathsf{Z}_0 = (\mathsf{P}^{\mathrm{a}})^{-1}\mathsf{Z}_0\Lambda \qquad \text{s.t.} \qquad \mathsf{Z}_0^{\mathrm{T}}(\mathsf{P}^{\mathrm{a}})^{-1}\mathsf{Z}_0 = \mathsf{I}\,, \tag{1}$$

where M is the tangent–linear model resolvent, C describes the final–time norm, and P^{a} is the analysis error covariance matrix (see, e.g., Barkmeijer et al. 1999). The set of vectors $\mathsf{Z}_t \equiv \mathsf{C}\mathsf{M}\mathsf{Z}_0$, that is, the time–evolved

structures Z_0, are the eigenvectors of the forecast error covariance matrix P^f. This fact can be seen, because operating with CMP^a on eq. (1) gives:

$$\Big(\mathsf{C}\underbrace{\mathsf{MP}^\mathsf{a}\Big)\mathsf{M}^\mathsf{T}}_{\equiv\mathsf{P}^\mathsf{f}}\mathsf{C}^\mathsf{T}\underbrace{\mathsf{CMZ}_0}_{\equiv\mathsf{Z}_\mathsf{t}} = \Big(\mathsf{CMP}^\mathsf{a}\Big)(\mathsf{P}^\mathsf{a})^{-1}\mathsf{Z}_0\Lambda\,, \tag{2}$$

which, with the definition of $\mathsf{P}^\mathsf{f} \equiv \mathsf{MP}^\mathsf{a}\mathsf{M}^\mathsf{T}$, yields the result:

$$\Big(\mathsf{CP}^\mathsf{f}\mathsf{C}^\mathsf{T}\Big)\,\mathsf{Z}_\mathsf{t} = \mathsf{Z}_\mathsf{t}\Lambda\,. \tag{3}$$

Eq. (3) states that the time–evolved HSVs Z_t are the eigenvectors of $\mathsf{CP}^\mathsf{f}\mathsf{C}^\mathsf{T}$, which is the forecast error covariance in the "final–time norm" C (see, Ehrendorfer and Tribbia 1997). Note that the following final–time orthogonality relationship is true for Z_t:

$$\mathsf{Z}_\mathsf{t}^\mathsf{T}\mathsf{Z}_\mathsf{t} = \Big(\mathsf{CMZ}_0\Big)^\mathsf{T}\Big(\mathsf{CMZ}_0\Big) = \mathsf{Z}_0^\mathsf{T}\underbrace{\mathsf{M}^\mathsf{T}\mathsf{C}^\mathsf{T}\mathsf{CMZ}_0} = \overbrace{\mathsf{Z}_0^\mathsf{T}(\mathsf{P}^\mathsf{a})^{-1}\mathsf{Z}_0}\Lambda = \Lambda\,, \tag{4}$$

where, for the second equality sign, eq. (1) is used. Thus, it is true that the final–time HSVs Z_t are orthogonal, with their squared length being equal to the squared singular values contained in the diagonal matrix Λ:

$$\mathsf{Z}_\mathsf{t}^\mathsf{T}\mathsf{Z}_\mathsf{t} = \Lambda\,. \tag{5}$$

It is apparent from the foregoing that the mathematical developments follow through even if approximations for P^a are used. One such approximation may be considered by constraining the SVs initially through an energy–like norm (see, e.g., Palmer et al. 1998); clearly, in that case the SVs and the appropriate SV–decomposition of P^a (see next subsection) need to be accordingly reinterpreted.

2.2 Uncertainty prediction: The SV–Decomposition of P^a

Since the initial–time HSVs satisfy eq. (1), it is true that P^a can be written as:

$$\mathsf{P}^\mathsf{a} = \mathsf{Z}_0\mathsf{Z}_0^\mathsf{T}\,. \tag{6}$$

Eq. (6) represents a special *square–root* for P^a that is different from an eigendecomposition and that is also not lower–triangular. The decomposition of P^a given in eq. (6) in terms of the initial time HSVs Z_0 is referred to as the *SV–decomposition of* P^a.

It is easily seen that under linear dynamics the SV–decomposition eq. (6) of P^a becomes the eigendecomposition of the forecast error covariance matrix, because operating on eq. (6) as given below, namely:

$$\Big(\mathsf{CM}\Big)\mathsf{P}^\mathsf{a}\Big(\mathsf{CM}\Big)^\mathsf{T} = \Big(\mathsf{CM}\Big)\mathsf{Z}_0\mathsf{Z}_0^\mathsf{T}\Big(\mathsf{CM}\Big)^\mathsf{T}, \tag{7}$$

yields:

$$\mathsf{CP}^\mathsf{f}\mathsf{C}^\mathsf{T} = \mathsf{Z}_\mathsf{t}\mathsf{Z}_\mathsf{t}^\mathsf{T}\,. \tag{8}$$

Further, augmenting eq. (8) by multiplying from the right with Z_t and observing the orthogonality relation eq. (5), yields:

$$\mathsf{CP}^\mathsf{f}\mathsf{C}^\mathsf{T}\mathsf{Z}_\mathsf{t} = \mathsf{Z}_\mathsf{t}\Lambda\,, \tag{9}$$

which is precisely eq. (3). Thus, we have established the result that for linear dynamics the SV–decomposition of P^a evolves into the eigendecomposition of P^f (see also, Ehrendorfer 1999b). The SV–decomposition given in eq. (6) forms the basis for the generation of initial–time perturbations in the multivariately normal sampling method implemented within the ECMWF Ensemble Prediction System (EPS). Again, if instead of P^a a simplified metric such as $\mathsf{C}^\mathsf{T}\mathsf{C}$ is used at initial time, the SV–decomposition will successively build up the corresponding matrix description of such a metric according to eq. (6).

2.3 Multinormal sampling based on the SV–decomposition of P^{a}

The basis for creating a set of multivariately normal perturbations is the fact that if the vector random variable $\mathbf{q}$ is standard multivariately normal:

$$\mathbf{q} \sim \mathcal{N}(0, \mathsf{I}) \,, \tag{10}$$

then the transformed variable $\mathbf{x}$ constructed through:

$$\mathbf{x} = \mathbf{x}_0^c + \mathsf{V}^{1/2}\mathbf{q} \tag{11}$$

will be multivariately normal with mean $\mathbf{x}_0^c$ and covariance structure V:

$$\mathbf{x} \sim \mathcal{N}(\mathbf{x}_0^c, \mathsf{V}) \tag{12}$$

(see, e.g., DeGroot 1986). The essential point underlying the singular vector–based multivariate normal sampling method is the recognition that the SV–decomposition eq. (6) represents an appropriate square–root of the analysis error covariance matrix that can be used advantageously in the construction process described through eq. (11). Specifically, if N SVs, computed according to eq. (1), are available, an (approximate) square–root of P^a is given, on the basis of eq. (6), by:

$$(\mathsf{P}^{\mathrm{a}})^{1/2} = \mathsf{Z}_0{}^{(N)} \,, \tag{13}$$

which is used in the sampling method, in analogy to eq. (11), to generate M perturbed states according to:

$$\mathbf{x}_i = \mathbf{x}_0^c + \mathsf{Z}_0^{(N)}\mathbf{q}_i \qquad i = 1, 2, ..., M \,. \tag{14}$$

Clearly, the $\mathbf{x}_i$ are multivariately normal with:

$$\mathbf{x} \sim \mathcal{N}\left(\mathbf{x}_0^c, (\mathsf{P}^{\mathrm{a}})^{(N)}\right) , \tag{15}$$

where:

$$(\mathsf{P}^{\mathrm{a}})^{(N)} \equiv \mathsf{Z}_0^{(N)}(\mathsf{Z}_0^{(N)})^{\mathrm{T}} \tag{16}$$

represents the approximation to P^{a} in terms of the SV–decomposition that is available on the basis of N SVs. Eq. (14), representing the heart of the singular vector–based multivariate normal sampling method, provides for a method that allows for generating M perturbations that are completely consistent with P^{a} knowledge, as described through a set of N SVs that satisfy (1). Clearly, the technique assumes that initial (analysis) errors are normally distributed. The attractive feature of the method is that for the linear regime the eigenvector properties of the evolved SVs will be exploited (see previous subsection, especially eq. (9)); further, as nonlinearity becomes important, the SV properties are taken into the nonlinear regime (see also, Gilmour et al. 2001).

Apparently, through eq. (14), the sampling method bears a strong resemblance to the operationally used *rotation* technique used at ECMWF (see, Molteni et al. 1996) that also creates perturbations to be added onto $\mathbf{x}_0^c$ as a linear combination of the available SVs. A technical point concerns establishing the overall magnitude of the multivariate normal perturbations $\mathsf{Z}_0^{(N)}\mathbf{q}_i$ (see eq. (14)) which is taken to be quite comparable to the magnitude prescribed in the rotation technique.

The methodology presented here allows from the beginning for the two free parameters N and M; that is, the possibility exists to generate an arbitrary number M of perturbed states from N SVs. In the presently used operational configuration of the rotation method in the ECMWF EPS, $N = 25$, and $M = 2 \times N$. Also, whereas the rotation method generates perturbed states that are exactly symmetric with respect to the control at initial time, this is not precisely the case for the sampling method. Clearly, however, such asymmetry is progressively reduced for increasing ensemble size M.

3 Results: Estimating variances and correlations

To investigate the performance of the sampling technique within the framework of the ECMWF EPS, ensemble experiments have been carried out. Specifically, these experiments are designed to address the impact of different configurations with regard to ensemble size M and the number of SVs N, used for approximating the analysis error covariance matrix at initial time. Sampling experiments have been carried out for selected dates during summer 2001, as well as December 2001. Emphasis has been given to the comparison of the sampling method with the operational rotation technique, as well as to the performance of ensembles with $M = 100$ members. A selection of these experiments is presented here to illustrate the error dynamics within the ECMWF EPS, as well as to study the potential benefit of the sampling technique in comparison to the operational rotation technique (see, Molteni et al. 1996).

The present operational ECMWF EPS is based on the so–called total–energy SVs rather than Hessian SVs (see, Palmer et al. 1998). In view of the theoretical properties of the HSVs (see section 2), this choice of initial–time metric, namely total energy, seems suboptimal. The computation of HSVs in a high–resolution EPS is, however, computationally very expensive and has yet to demonstrate a significant impact on the performance of the forecast (see, Barkmeijer et al. 1998, Barkmeijer et al. 1999).

3.1 Variances estimated from EPS integrations

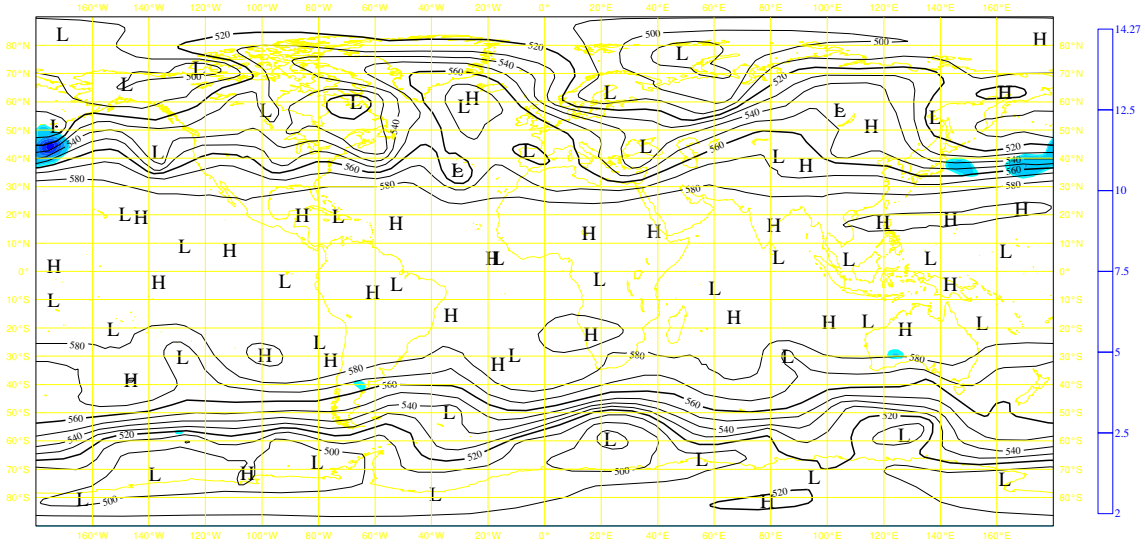

Figure 1: **D+0 sampling experiment with M=50/N=25**. *Initial time (20011219/1200) temperature variance (unit K^2) at 850hPa (shaded; contour interval indicated on right–hand–side of figure). Contours show Z500 height field (unit 10 m) of control forecast.*

As an example for the error dynamics in the ECMWF EPS, results from a sampling experiment with starting date 20011219/1200 are presented in Figs. 1 – 6. In the results shown in Figs. 1 – 4, $M = 50$ perturbations are *sampled* from $N = 25$ SVs; thus, this choice of parameters mimics the operational configuration. Figs. 1 – 4 show temperature variances in units of K^2 at 850hPa at four different times. Shown in contours is the 500hPa geopotential height field (unit 10m) of the control forecast. The contour interval for the variances is given on the right–hand–side of the figures (regions with variances greater than 2 K^2 are shaded). It is seen from Fig. 1 that the (nonzero) variance structures are associated with regions of strong cyclonic activity and that the largest variance obtained is about 10 K^2 (at 175^{o}W). Over the first 24 hours of the forecast the error

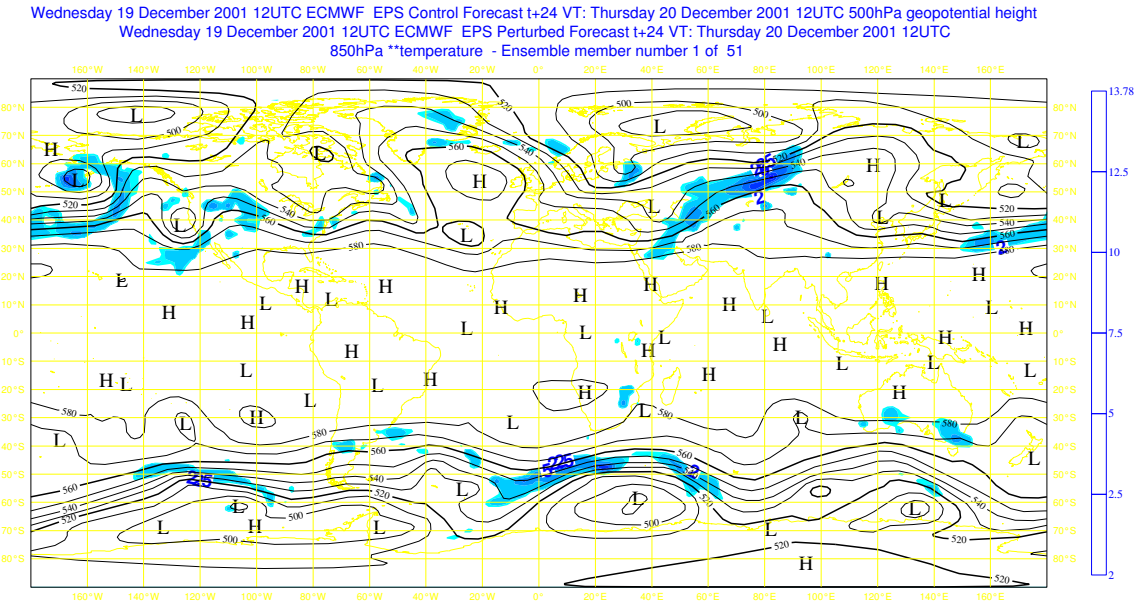

Figure 2: **D+1 sampling experiment with M=50/N=25**. *As Fig. 1, but for D+1 forecast.*

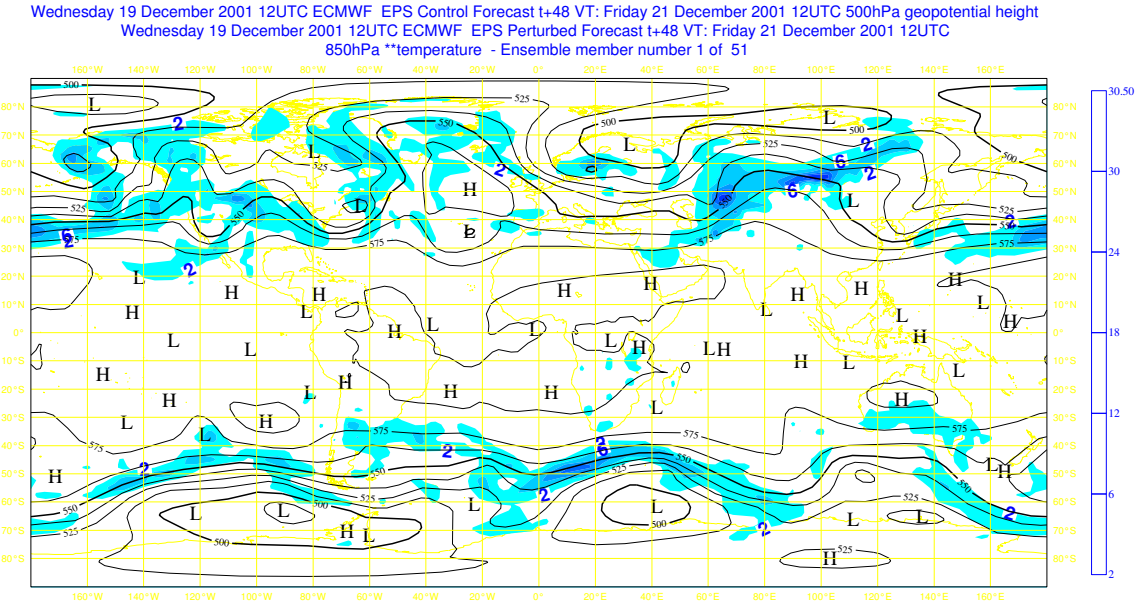

Figure 3: **D+2 sampling experiment with M=50/N=25**. *As Fig. 1, but for D+2 forecast.*

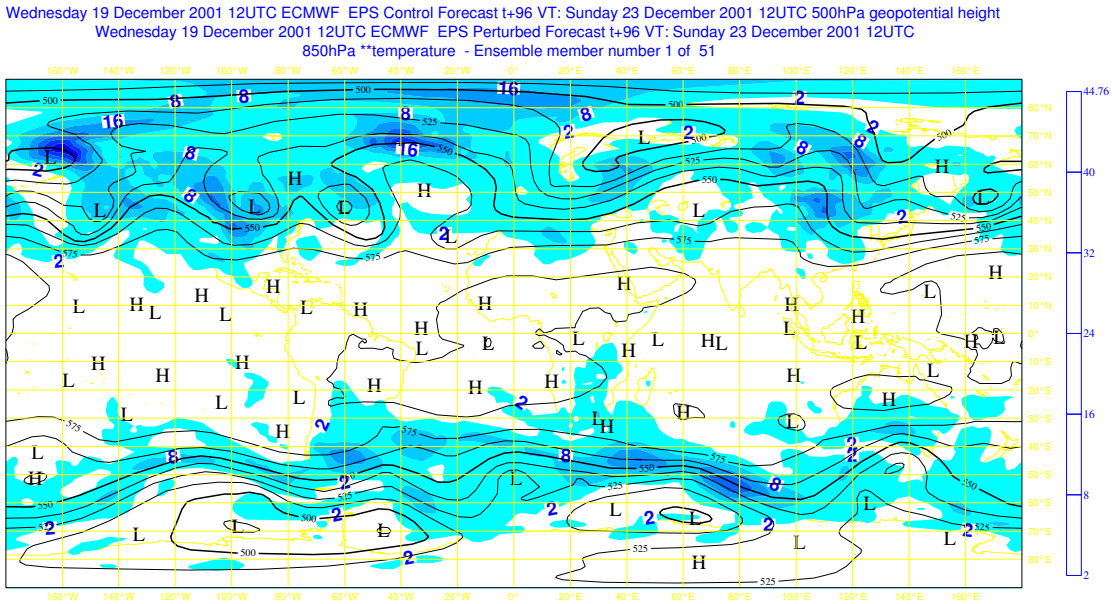

Figure 4: **D+4 sampling experiment with M=50/N=25**. *As Fig. 1, but for D+4 forecast.*

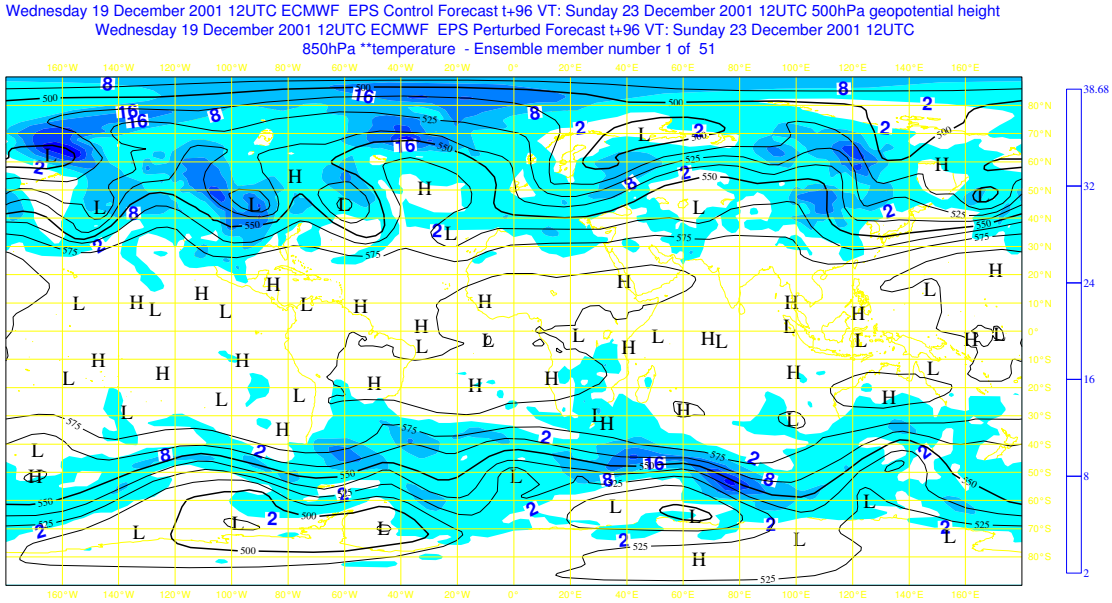

Figure 5: **D+4 operational EPS experiment with N=25**. *As Fig. 1, but for D+4 forecast, as obtained with operational ECMWF EPS.*

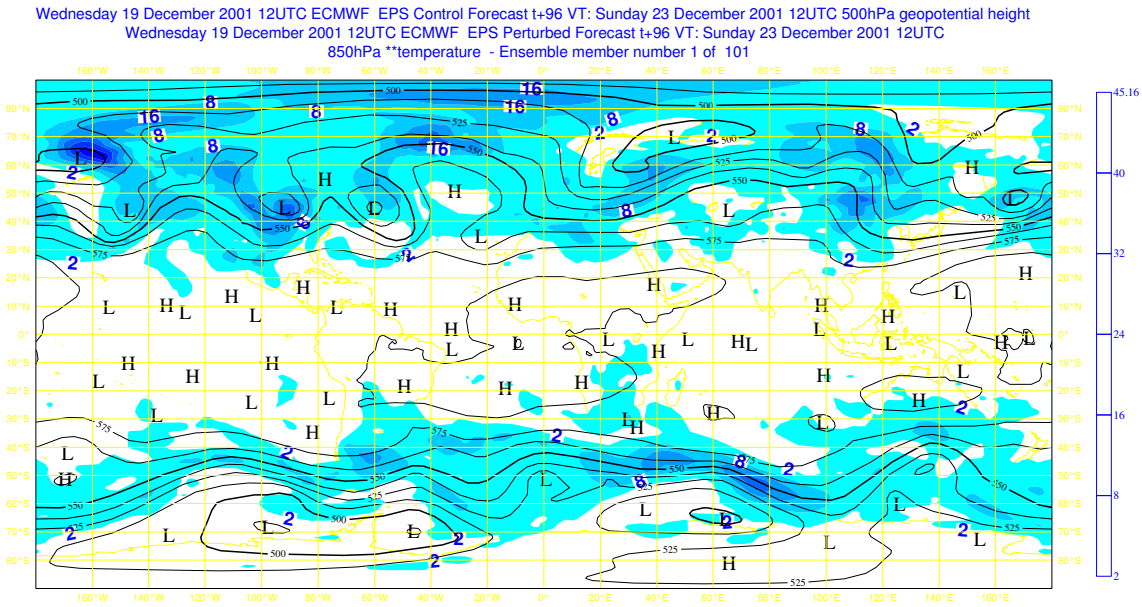

Figure 6: **D+4 sampling experiment with M=100/N=50**. *As Fig. 4, but for sampling experiment with M=100/N=50 starting from 20011219/1200.*

growth is fairly small in terms of absolute values, but the variance structures are spreading substantially, thus covering the baroclinic regions of the individual cyclones across the globe (Fig. 2). Growth further into the forecast (Figs. 3 and 4) shows that the largest variance is associated with the cyclone over the north–east Pacific (about 60^oN, 170^oW), showing variances of about 30 K^2 at D+2 and almost 45 K^2 into the forecast range at D+4, respectively. Hence, the error doubling time is estimated to be slightly larger than 2 days. The spatial structure of the variance fields at D+2 and D+4 still shows the largest variances corresponding to regions of cyclonic activity, but variances between 2 K^2 and 8 K^2 are covering most of the extratropics.

For comparison with the operational EPS configuration, D+4 temperature variances at 850hPa, as estimated from the operational ECMWF EPS, are shown in Fig. 5, for the same initial date as used in Figs. 1 – 4. Comparing Fig. 5 with Fig. 4 reveals that the error variances are smaller in the operational run, compared to the corresponding sampling experiment. The two figures are very similar in an overall sense; however, the structures associated with the largest variances have a larger magnitude in the sampling experiment shown in Fig. 4. D+4 temperature variances at 850hPa from a sampling experiment using $M = 100$ ensemble members on the basis of $N = 50$ SVs are shown in Fig. 6. It is evident that again the structures for D+4 variances (in Fig. 6) are quite similar, compared to both Figs. 4 and 5. Evidently, this comparison with the operational rotation technique in terms of variances provides evidence for the robust performance of the SV–based multinormal sampling technique.

3.2 Correlations estimated from EPS integrations

Having illustrated in section 3.1 the degree to which variances are different when perturbed integrations are carried out within the ECMWF EPS, with perturbations created either through the operational rotation technique or through the sampling method, attention is now turned to the estimation of off–diagonal elements of the forecast error covariance matrix, in terms of correlations. Maps of 500hPa geopotential–height correlations of one particular gridpoint (50^oN, O^oE) with all other gridpoints on the globe are shown in Figs. 7 – 9. Correlations shown in these figures are valid for D+4 forecasts and are estimated from EPS ensemble forecasts starting from

20011219/1200.

Fig. 7, showing correlation structures based on the operational EPS forecast, illustrates that estimating off–diagonal elements of the forecast error covariance matrix P^{f} from only $M = 50$ ensemble members gives highly unrealistic correlation structures. Fig. 7 suggests that geopotential height of one point over Europe (i.e., 50^oN, O^oE) is highly correlated with geopotential height over Australia and the South Pacific. Obviously, such correlations are highly unrealistic in the real atmosphere and are simply the result of a systematic undersampling of the correlation structure. To overcome this undersampling problem the number of ensemble members apparently has to be increased. However, it is evident from Fig. 8 that the correlations can be improved substantially on the basis of only $M = 50$ EPS members if the *sampling technique* is used for the generation of the initial perturbations. Completely analogous to Fig. 7, Fig. 8 shows Z500 correlations that are now estimated from a sampling experiment using $M = 50$ members (and $N = 25$ SVs). This improvement in the estimation of off–diagonal elements is considered to be due to the fact that the operational rotation technique (underlying the results in Fig. 7) imposes strictly symmetric perturbations with opposite sign at the initial time (see, Molteni et al. 1996).

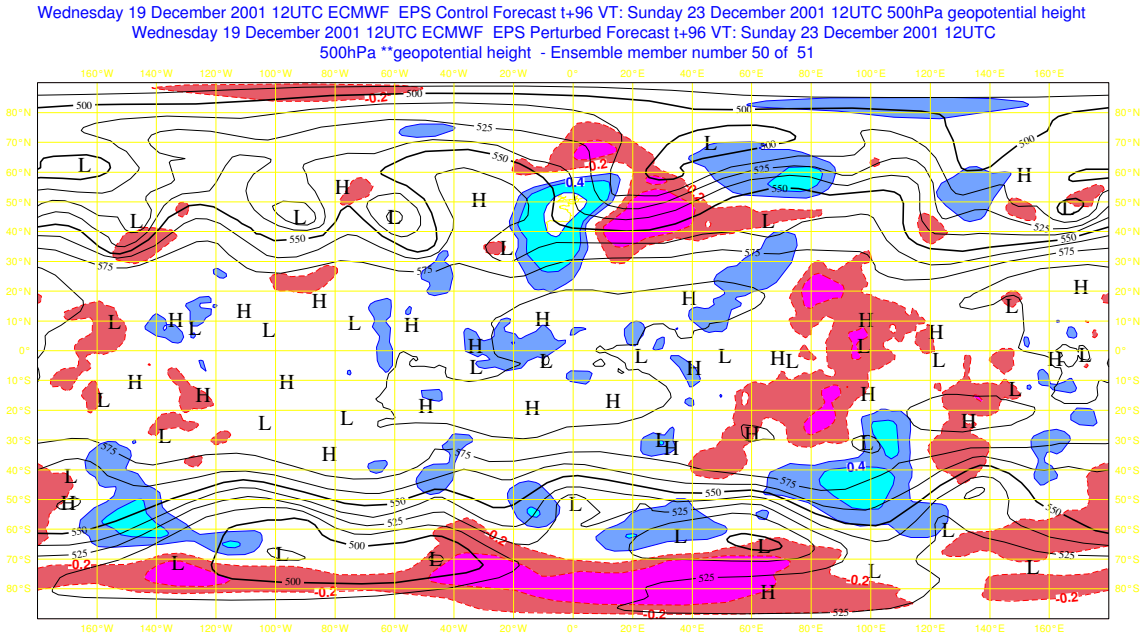

Figure 7: D+4 geopotential–height correlations at 500hPa (of grid point 50^oN and O^oE with all other grid points on the globe) obtained from ECMWF operational EPS forecast starting from 20011219/1200. Also shown is Z500 height field of control forecast (black contours; unit 10m).

Finally, Fig. 9 again shows Z500 correlations based on an EPS sampling experiment, but now for the situation that the sampling method uses $M = 100$ members on the basis of $N = 50$ SVs. It is evident from Fig. 9 that this configuration ensures that the unrealistic correlation structures found in the previous figures largely disappear; that is, Fig. 9 does not show any significant correlations with points in the southern hemisphere. These comparisons of the sampling and the rotation technique seem to be slightly favorable for the sampling technique, in terms of its efficiency to remove unrealistic correlations, given the constraint that M perturbed states can be integrated forward in time.

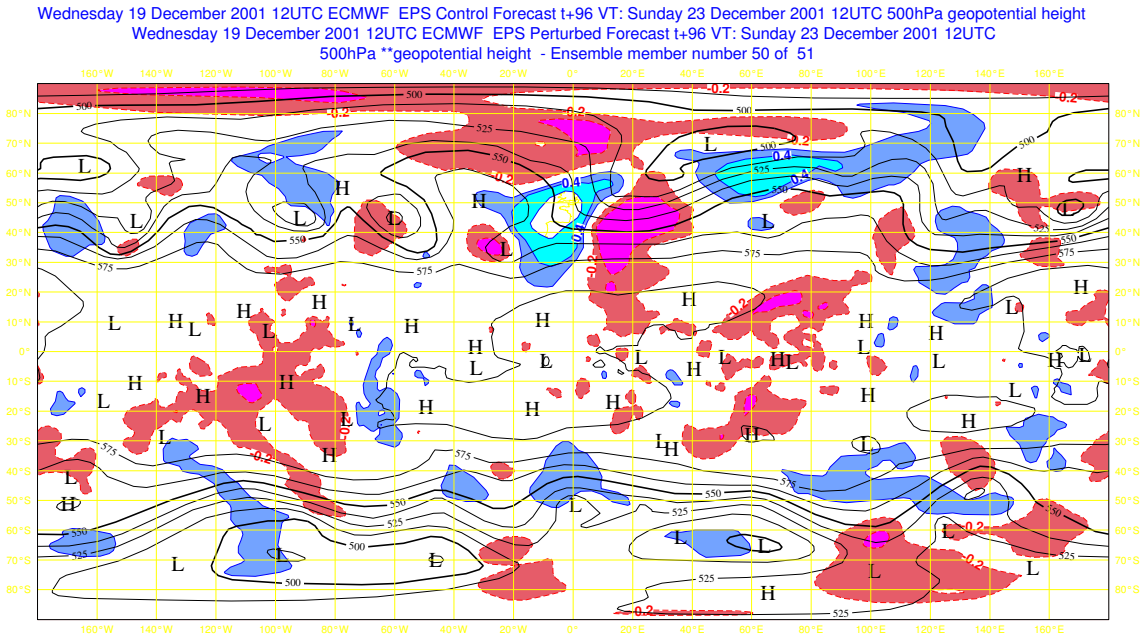

Figure 8: As Fig. 7, but for EPS sampling experiment with $M = 50$ members based on $N = 25$ SVs, starting from 20011219/1200.

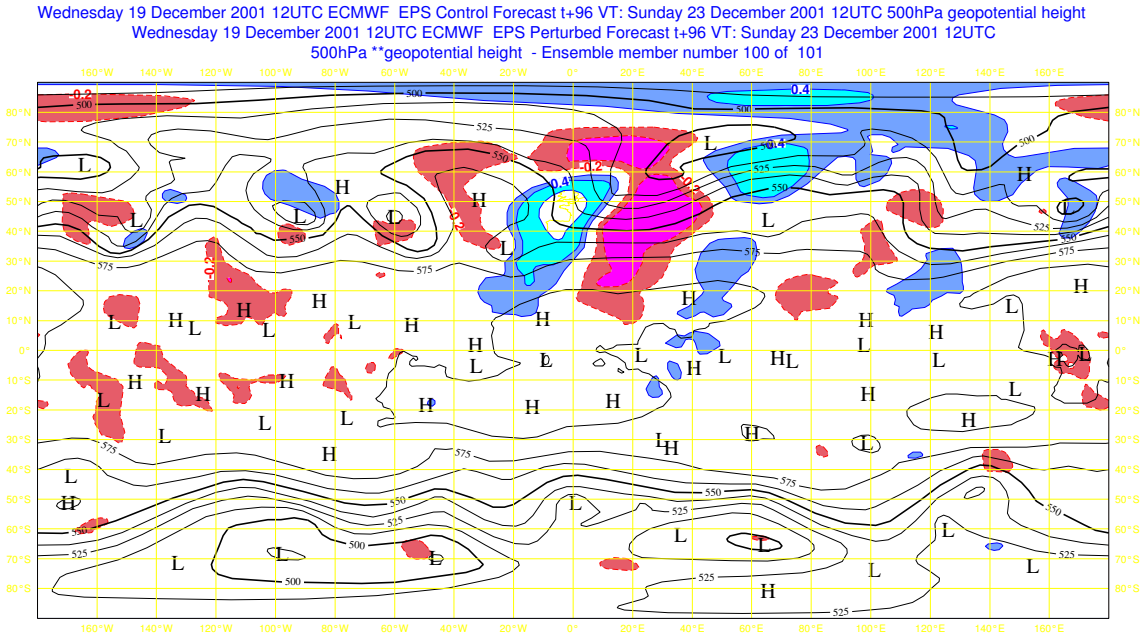

Figure 9: As Fig. 7, but for EPS sampling experiment with $M = 100$ members based on $N = 50$ SVs, starting from 20011219/1200.

4 Results: Performance in terms of EPS scores

Given the performance of the sampling method in comparison to the operational EPS rotation method in terms variances and correlations (see section 3), a few selected skill measures of both techniques are compared here. With regard to the verification of probability forecasts reference is made to the excellent book by Wilks (1995).

Fig. 10 shows the Z500 anomaly correlation, as well as RMS error (unit m) of the ensemble mean computed with respect to the control forecast and evaluated for the northern hemisphere. The curves correspond to the operational EPS (red), and sampling experiments with $M = 50/N = 25$ (blue), with $M = 50/N = 50$ (green), and with $M = 100/N = 50$ (black), respectively. All curves are computed as means over 8 cases in December 2001. The top panel in Fig. 10 shows the difference in skill between the ensemble mean and the control forecast. The lower panel shows the corresponding difference in RMS errors between the ensemble mean and the control. It is evident from Fig. 10 that after D+3 the ensemble mean is more skillful than the control forecast. Moreover, the ensemble mean of the sampling experiments performs slightly better after D+6.

Another measure of the performance of the EPS is given by the area under the Relative Operating Characteristic (ROC) curve, which is an overall measure of the quality of an ensemble forecast. Basically, it is a generalization of the concept of contingency tables to probabilistic forecasts. A ROC area of one indicates a perfect forecast, and a value of 0.5 is considered to be the lower bound for a useful forecast. For a detailed description of the properties of this verification measure, reference is made to Stanski et al. (1989). Fig. 11 shows the ROC area curve for the same experimental configurations as in Fig. 10 (also with the same colouring conventions). Curves shown correspond to temperature at 850 hPa for the event that the temperature anomaly is greater than 8K evaluated over the northern hemisphere. It is evident from Fig. 11 (upper panel) that all EPS configurations behave quite similar in terms of ROC area. The lower panel in Fig. 11 shows the change in ROC area with respect to the operational EPS, and indicates a slight improvement for the sampling experiments with configurations $M = 50/N = 50$ (green curve) and $M = 100/N = 50$ (black curve), apparently resulting from larger sampling size combined with more detailed SV knowledge.

Fig. 12 shows Brier (see, Brier 1950) scores (BSs), as well as Brier skill scores (BSS) for the same EPS configurations as in the previous figures. As in Fig. 11, the verification area is the northern hemisphere and statistics are shown for T850 for the event that the temperature anomaly is greater than 8K. The BS is essentially a mean–squared error for probability forecasts, verified for subsequent binary events (i.e., whether or not the specified event did happen). The BSS is a skill score computed for the BS with respect to climatology. Thus, BSS=1 indicates a perfect forecast, and BSS=0 indicates no improvement compared to climatology. Fig. 12 suggests that in terms of BSS all sampling configurations perform very similar, also in comparison to the operational EPS.

A final verification statistic is shown in Fig. 13, displaying the number of outliers computed for six verification areas for sampling experiments with different choices of M and N (same colouring conventions as before), as well as for the operational EPS (red curve). The basic idea of this verification statistic is that the M ensemble members are used to partition the real line into distinct intervals. Then, assuming that the evolving ensemble members provide a random sample of evolving probability density function, and neglecting model errors, each interval is equally likely to contain the analysis (averaged over the verification area). For details refer to Strauss and Lanzinger (1996) and Buizza (1997). Fig. 13 shows the percentage of outliers for T850 relative to the expected value of $100\% \times 2/(M+1)$. It is evident that the sampling technique reduces the number of outliers for all configurations. The largest reduction is obtained for the ensemble using $M = 100$ members. Interestingly, the sampling configuration using $M = 50$ members on the basis of $N = 50$ (green curve) SVs performs almost as well as the configuration $M = 100/N = 50$ (black curve). This result is probably due to the fact that including a larger number of SVs leads to more detailed large–scale error structures and thus to lower probabilities for the analysis to be lying outside of the two extremes of the ensemble.

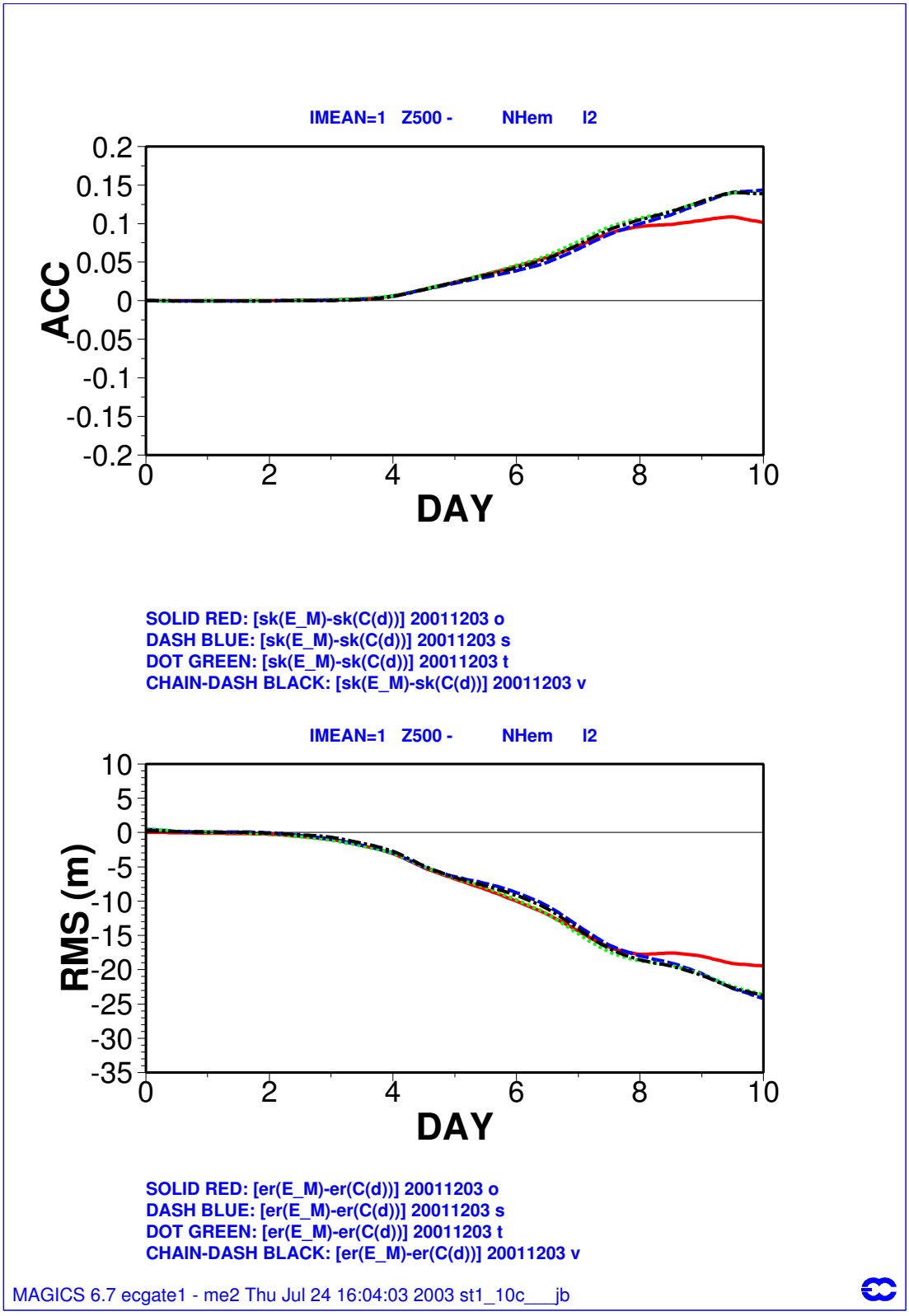

Figure 10: Z500 anomaly correlation (top panel) and RMS error (unit m; lower panel) of the ensemble mean with respect to the control forecast as function of forecast day computed for the northern hemisphere (mean over 8 cases); operational EPS (red), sampling $M = 50/N = 25$ (blue), sampling $M = 50/N = 50$ (green), sampling $M = 100/N = 50$ (black).

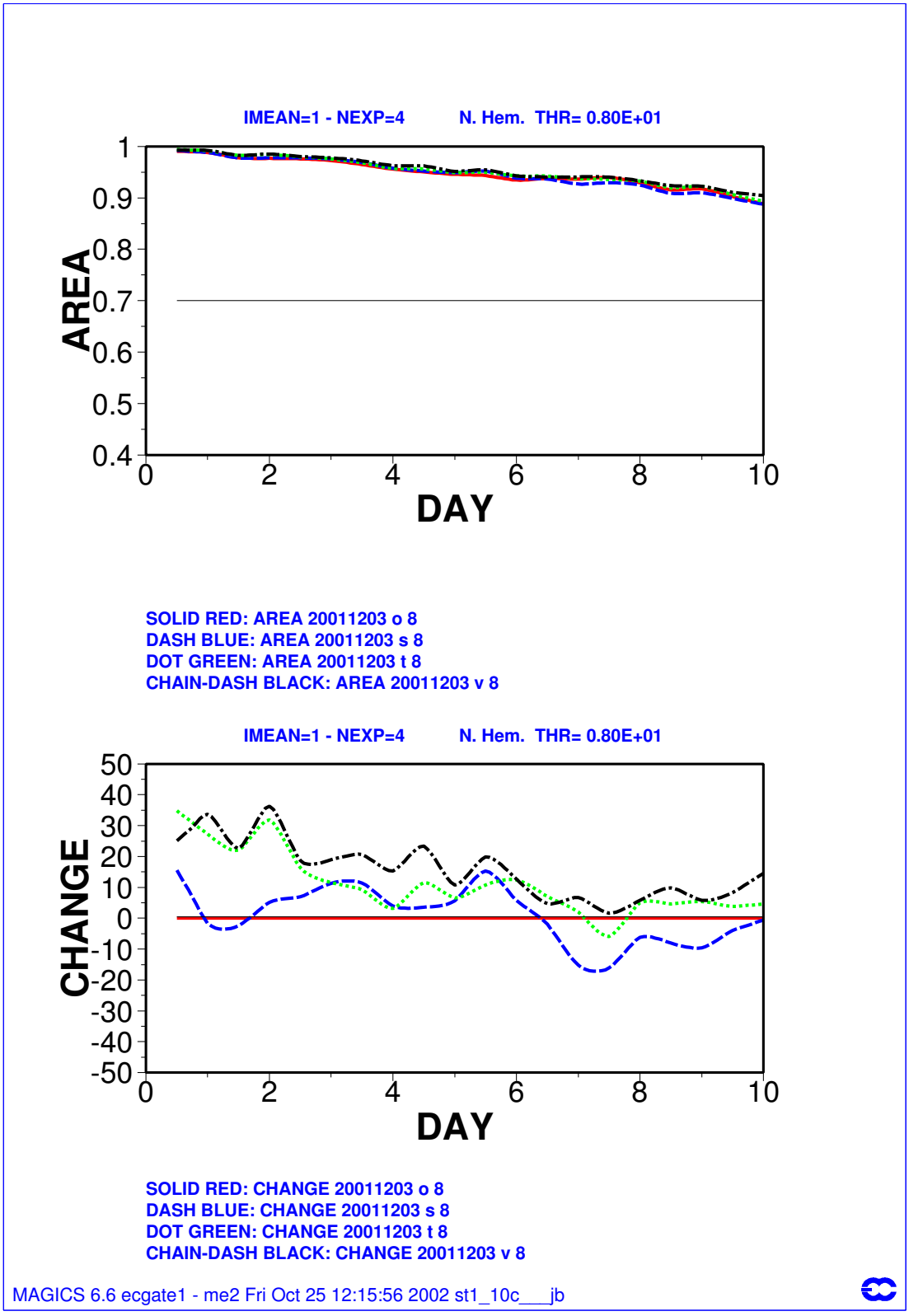

Figure 11: T850 ROC area (top panel) and relative change with respect to the operational EPS (lower panel) for the threshold 8K computed for northern hemisphere (mean over 8 cases); operational EPS (red), sampling $M = 50/N = 25$ (blue), $M = 50/N = 50$ (green), and $M = 100/N = 50$ (black).

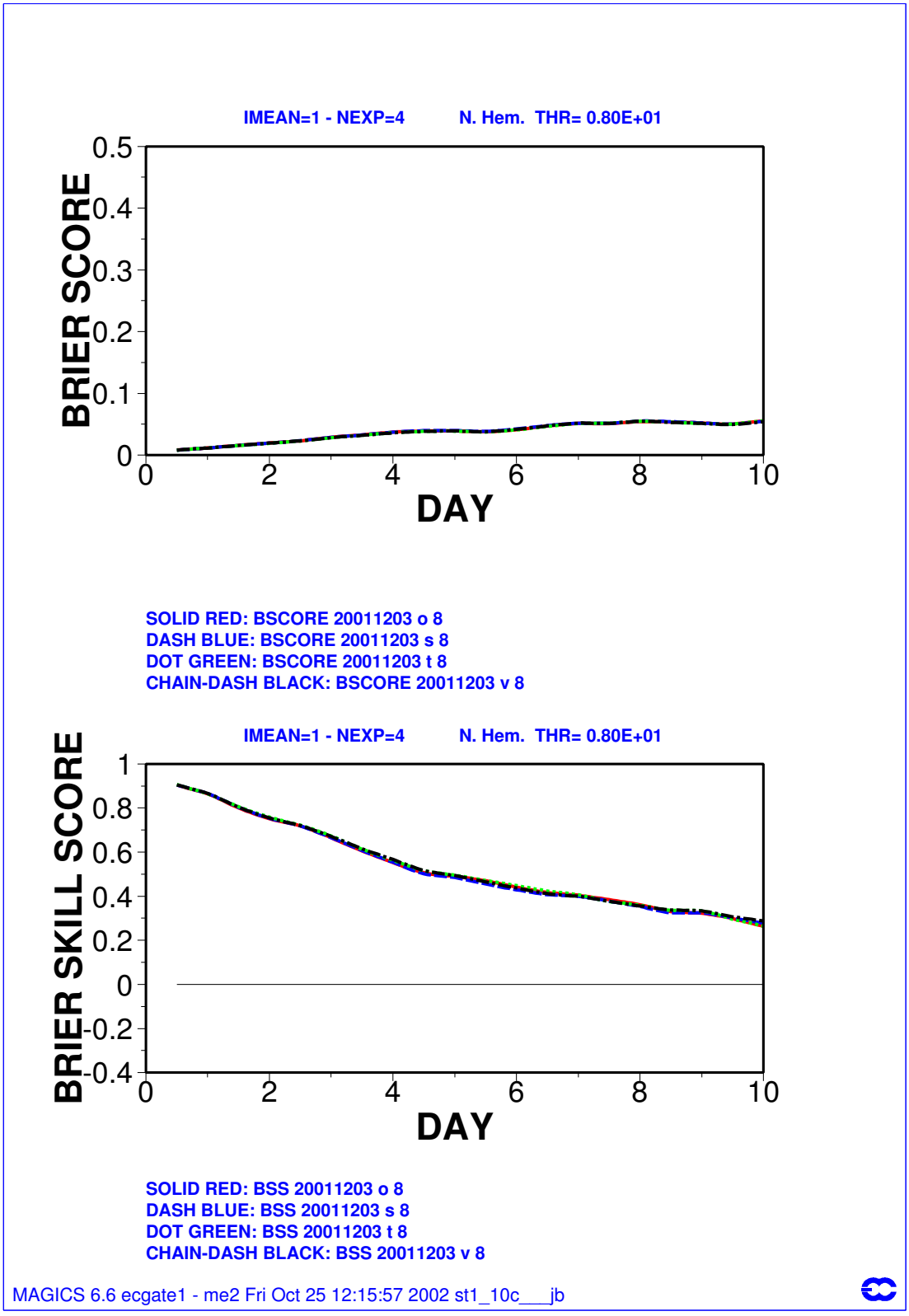

Figure 12: Brier score (top panel) and Brier skill score (lower panel) for T850 for the threshold 8K computed for the northern hemisphere (mean over 8 cases): operational EPS (red), sampling $M = 50/N = 25$ (blue), $M = 50/N = 50$ (green), and $M = 100/N = 50$ (black).

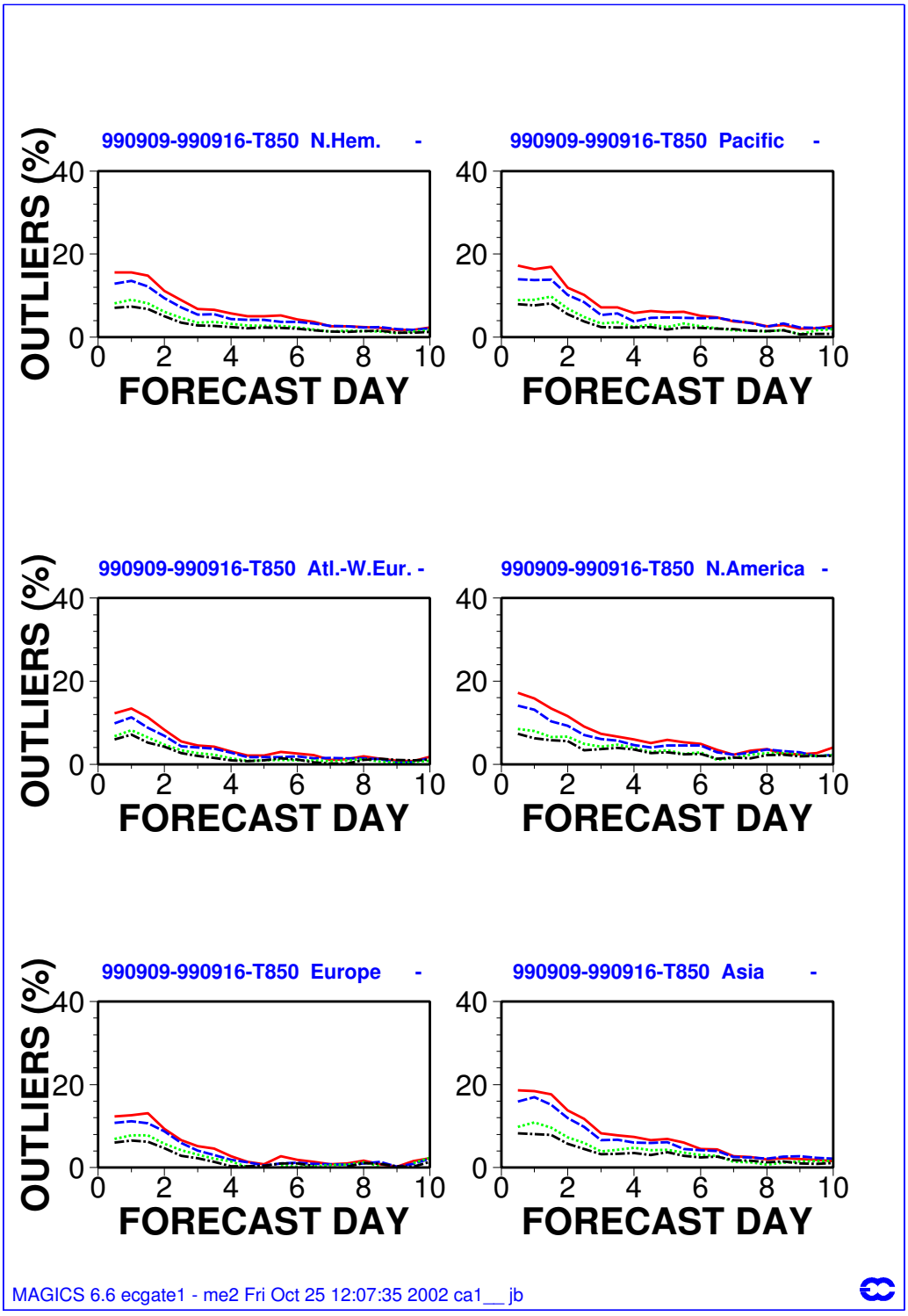

Figure 13: Relative number of outliers for T850 for 6 verification areas as indicated (mean over 8 cases): operational EPS (red), sampling $M = 50/N = 25$ (blue), $M = 50/N = 50$ (green), and $M = 100/N = 50$ (black).

5 Related research

Further work carried out in Special Project SPATME01 concerns the impact of dynamic background information on the quality of subsequent analyses. Work in this direction was carried out within the ECMWF assimilation system; code is in existence that allows for computing within the ECMWF assimilation system the complete analysis error covariance matrix at T21/L3 resolution (through inverting the Hessian of the variational cost function; see Fisher and Courtier 1995), to propagate these analysis errors using quasigeostrophic (QG) dynamics, and to interface that result back into the next assimilation step of the full system. Details for this QG extended Kalman Filter (EKF) are found in, for example, Ehrendorfer et al. (2001), Ehrendorfer (2000a), Ehrendorfer (1999a), Ehrendorfer and Bouttier (1998).

One of the primary products of this QG/EKF are analysis and forecast error covariance matrices for vorticity. The analysis error covariance matrices are evolved over time according to the complete prediction equation of the EKF, using the QG dynamics of the model by Marshall and Molteni (1993). An example of such a (tangent–linear) time evolution over 48 hours is shown in Figs. 14 and 15. Fig. 14 shows the time–evolved forecast error variances when 100 (out of the 1449 possible) SVs are used in the prediction equation. Fig. 15 shows the complete result obtained with all SVs. The SVs used here were computed using the analysis error covariance as initial constraint, and the total energy norm, described by Ehrendorfer (2000b), as the final constraint. The optimal reconstruction of the forecast error covariance (at final) time is based on the SV–decomposition (described by Ehrendorfer 1999a, Ehrendorfer 1999b; see also section 2). From Figs. 14 and 15 it becomes evident that the forecast error variances are, in terms of their structure, well described when only 100 SVs are used. The 100 SVs describe 22.91% of the variance at the initial time and 64.99% of the variance at the final time.

In a parallel data assimilation effort (see, Beck 2003, Ehrendorfer et al. 2003) assimilation experiments were carried out within an assimilation system entirely contained within the QG model dynamics formulated by Marshall and Molteni (1993). As illustrated schematically in Fig. 16, the central part is a four–dimensional variational (4D–Var) system that, given appropriate input, produces an analysis, together with $\mathbf{P}^a$. As indicated, three options exist within this system for time–evolving $\mathbf{P}^a$.

One of the major results of that investigation is shown in Fig. 17. In this investigation, the background error covariance matrix is made (partially) dynamic (through the choice of the "middle" option in Fig. 16) by computing the time evolution of the analysis error covariance matrix on the basis of the HSVs along the theory of the Reduced–Rank Kalman Filter (e.g., Fisher and Andersson 2001). Results from the simulation experiments within the QG assimilation system shown in Fig. 17 demonstrate clearly that increasing the amount of flow–dependence (through including successively more HSVs) in the background error covariance matrix leads to a positive impact on analysis quality in this assimilation system. In Fig. 17 the black curve shows analysis and forecast errors for static background information, whereas the orange curve shows the "ideal" situation of the fully flow–dependent background error covariance matrix computed according to Kalman filter theory. In between, results are shown for including 10, 100, 200, and 1000 HSVs (out of a total of 1449 HSVs). The improvement in analysis quality that is expected from theory can be demonstrated in this system.

6 Conclusions

In conclusion, in the work related to this Special Project emphasis has been on both data assimilation and ensemble prediction. While data assimilation evidence is preliminary and restricted to simplified (i.e., quasi-geostrophic) dynamics, results from the sampling method within the ECMWF EPS clearly demonstrate that the sampling method possesses no disadvantages as compared to the presently operationally–used rotation method.

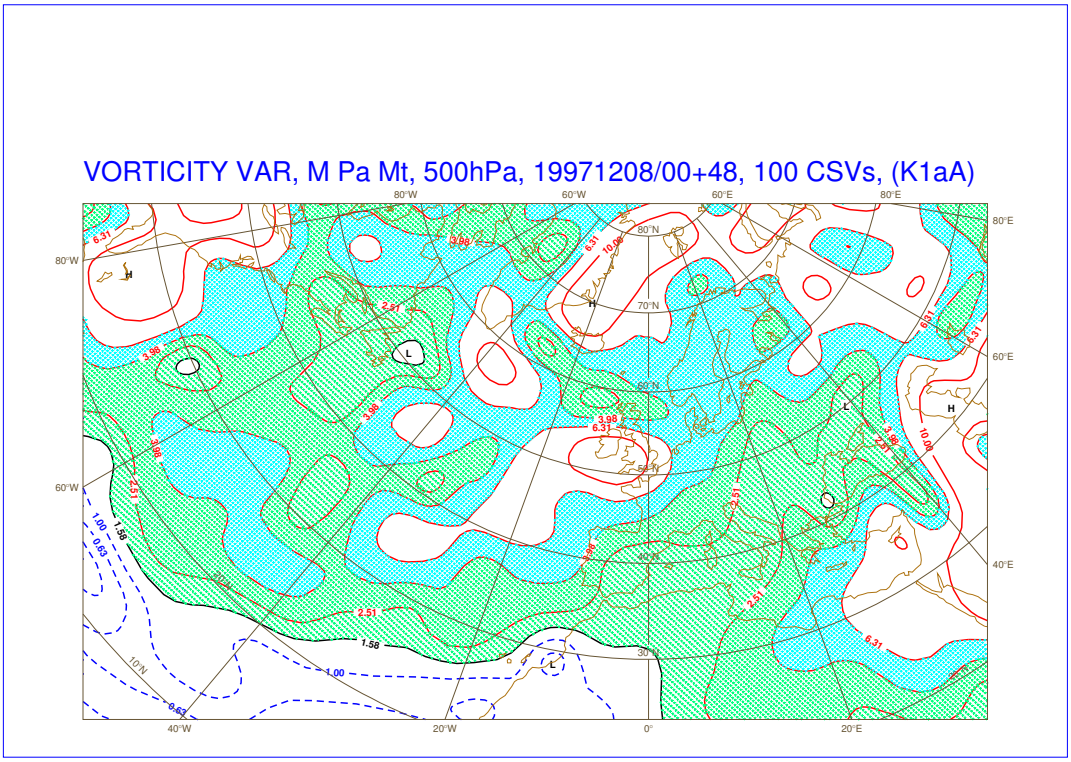

Figure 14: Forecast error variances as obtained by 48–hour tangent–linear prediction (with quasigeostrophic dynamics), based on complete Kalman filer prediction equation, started from analysis error covariance matrix described by 100 SVs. Units are $10^{-11}s^{-2}$*. These 100 SVs describe 22.91% of the analysis error variance (at the initial time) and 64.99% of the forecast error variance.*

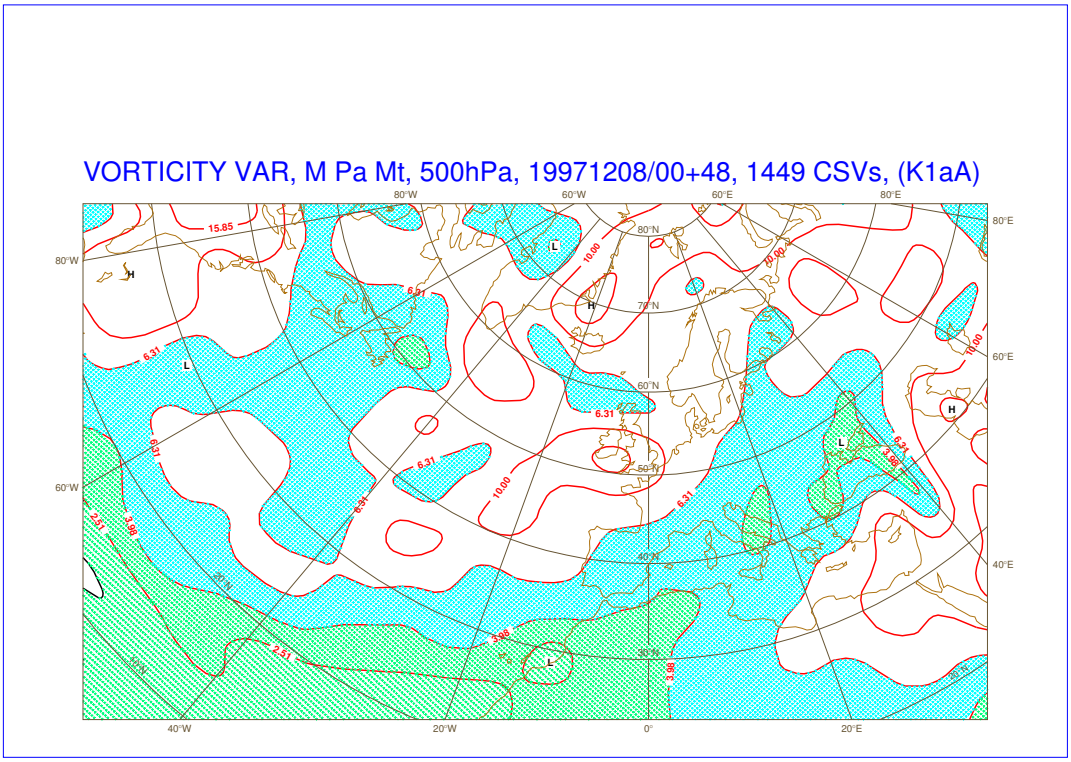

Figure 15: Same as Fig. 14, except for all 1449 SVs.

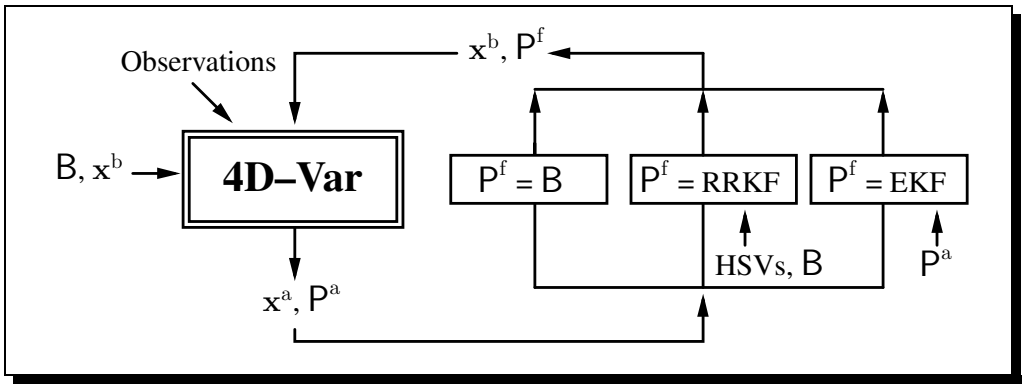

Figure 16: Illustration of the QG/4D–Var system. Note that loop indicated by arrows symbolizes cycling experiment. The three different branches correspond to options for specifying $\mathbf{P}^f$.

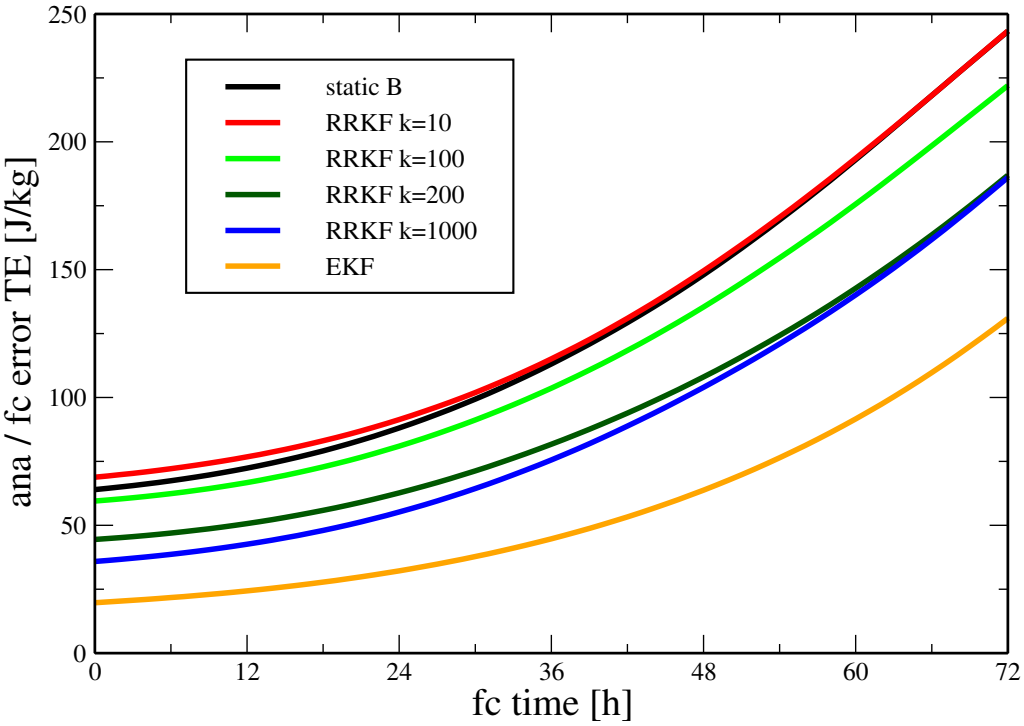

Figure 17: Performance of the QG/4D–Var system in terms of analysis and forecast error as a function of lead time; see text for additional details. Taken from Beck (2003).

Further, the sampling method is already part of the ECMWF Integrated Forecasting System, is derived from a strong statistical basis, and may be a particularly attractive method when norms specifically describing analysis error are introduced to constrain the SV computation at the initial time.

Acknowledgements

The hospitality of ECMWF during visits in the context of this Special Project is gratefully acknowledged. It is our particular pleasure to express our gratitude to Drs. A. Hollingsworth and T.N. Palmer for continued support of this project. We specifically acknowledge the help of Drs. Roberto Buizza and Jan Barkmeijer in using the EPS and its verification software. Much of the material in sections 3 and 4 is taken from Beck (2003). We thank Prof. Dr. M. Kuhn, Head of the Institute for Meteorology and Geophysics, University of Innsbruck, and Prof. Dr. R. Steinacker, Head of the Institute for Meteorology and Geophysics, University of Vienna, for the possibility to use the infrastructure of the Institutes during this project. We thank Dr. F. Molteni for generously providing the quasigeostrophic model code. We thank the Central Institute for Meteorology and Geodynamics, Vienna, for support in the context of this ECMWF Special Project. Financial support through ECMWF and through the FWF (Austrian Science Foundation) Project Grant P13729–GEO to enable this work is gratefully acknowledged.

References

Barkmeijer, J., R. Buizza, and T. Palmer, 1999: 3D-Var Hessian singular vectors and their potential use in the ECMWF Ensemble Prediction System. *Quart. J. Roy. Meteor. Soc.*, **125**, 2333–2351.

Barkmeijer, J., M. van Gijzen, and F. Bouttier, 1998: Singular vectors and estimates of the analysis–error covariance metric. *Quart. J. Roy. Meteor. Soc.*, **124**, 1695–1713.

Beck, A., 2003: Data assimilation and covariance dynamics in atmospheric models. Doctoral Dissertation, Fakultät für Naturwissenschaften und Mathematik, University of Vienna, pp. viii+105.

Brier, G.W., 1950: Verification of forecasts expressed in terms of probability. *Mon. Wea. Rev.*, **78**, 1–3.

Buizza, R., 1997: Potential forecast skill of ensemble prediction and spread and skill distributions of the ECMWF ensemble prediction system. *Mon. Wea. Rev.*, **125**, 99–119.

Buizza, R., and T.N. Palmer, 1995: The singular–vector structure of the atmospheric global circulation. *J. Atmos. Sci.*, **52**, 1434–1456.

DeGroot, M.H., 1986: *Probability and Statistics*. Addison-Wesley, 723 pp.

Ehrendorfer, M., 1999a: Kalman filtering and atmospheric predictability. In: *Proceedings ECMWF Workshop on Diagnosis of Data Assimilation Systems, 2 – 4 November 1998*, pp. 29–43.

Ehrendorfer, M., 1999b: Prediction of the uncertainty of numerical weather forecasts: Problems and approaches. In: *Proceedings ECMWF Workshop on Predictability, 20 – 22 October 1997*, pp. 27–99.

Ehrendorfer, M., 2000a: An exact extended Kalman filter based on quasigeostrophic dynamics. In: *Proceedings of the Third WMO International Symposium on Assimilation of Observations in Meteorology and Oceanography, Québec City, Canada, 7–11 June 1999*, pp. 375–378. WMO Technical Document WMO/TD - No. 986.

Ehrendorfer, M., 2000b: The total energy norm in a quasigeostrophic model. *J. Atmos. Sci.*, **57**, 3443–3451.

Ehrendorfer, M., A. Beck, and P. Haas, 2003: End of Project Report 1999–2002 for FWF Project P13729–GEO "Variational Data Assimilation and Ensemble Prediction". 214 pp. [Available from martin.ehrendorfer@uibk.ac.at, also available at meteo.uibk.ac.at].

Ehrendorfer, M., and F. Bouttier, 1998: *An explicit low–resolution extended Kalman filter: Implementation and preliminary experimentation*. ECMWF Tech. Memo. No. 259, 21 pp. [Available from ECMWF, Shinfield Park, Reading RG2 9AX, England].

Ehrendorfer, M., T.N. Palmer, and F. Bouttier, 2001: Analysis and forecast error covariances in an exact Kalman filter. In: *Research Activities in Atmospheric and Oceanic Modeling*, H. Ritchie (Ed.), Volume No. 31, WMO/TD-No. 1064, pp. 1.17–1.18. WMO.

Ehrendorfer, M., and J.J. Tribbia, 1997: Optimal prediction of forecast error covariances through singular vectors. *J. Atmos. Sci.*, **54**, 286–313.

Farrell, B.F., and P.J. Ioannou, 1996: Generalized stability theory. Part I: Autonomous operators. *J. Atmos. Sci.*, **53**, 2025–2040.

Fisher, M., and E. Andersson, 2001: *Developments in 4D–Var and Kalman Filtering*. ECMWF Tech. Memo. No. 347, 36 pp. [Available from ECMWF, Shinfield Park, Reading RG2 9AX, England].

Fisher, M., and P. Courtier, 1995: *Estimating the covariance matrices of analysis and forecast error in variational data assimilation*. ECMWF Tech. Memo. No. 220, 26 pp. [Available from ECMWF, Shinfield Park, Reading RG2 9AX, England].

Gilmour, I., L.A. Smith, and R. Buizza, 2001: Linear regime duration: Is 24 hours a long time in synoptic weather forecasting? *J. Atmos. Sci.*, **58**, 3525–3539.

Marshall, J., and F. Molteni, 1993: Toward a dynamical understanding of planetary-scale flow regimes. *J. Atmos. Sci.*, **50**, 1792–1818.

Molteni, F., R. Buizza, T.N. Palmer, and T. Petroliagis, 1996: The ECMWF ensemble prediction system: Methodology and validation. *Quart. J. Roy. Meteor. Soc.*, **122**, 73–119.

Palmer, T.N., R. Gelaro, J. Barkmeijer, and R. Buizza, 1998: Singular vectors, metrics, and adaptive observations. *J. Atmos. Sci.*, **55**, 633–653.

Stanski, H., L. Wilson, and W. Burrows, 1989: Survey of common verification methods in meteorology. Report No. 89–5, Atmospheric Environment Service, Forecast Research Division, 4905 Dufferin Street, Downsview, Ontario, Canada M3H 5T4.

Strauss, B., and A. Lanzinger, 1996: Validation of the ECMWF Ensemble Prediction System. In: *Proceedings ECMWF Seminar on Predictability, Vol. II, 4 – 8 September 1995*, pp. 157–166.

Wilks, D.S., 1995: *Statistical Methods in the Atmospheric Sciences*, Volume 59 of *International Geophysics Series*. Academic Press, 467 pp.

A Technical description of sampling technique

The sampling technique has been implemented within the IFS in April 2000 and is available from IFS model cycle 22R3 onwards. The implementation affects two subroutines (*comp_rotmat.f, comp_rotpert.f*), one SMS script (*rot.sms*), as well as minor modifications to prepIFS. The changes to the individual components, as well as the specifications in prepIFS are described briefly in the following subsections.

Note that the implementation ensures that the results are **reproducible** in the sense that for one particular initial date and number of ensemble members M the same perturbations are obtained when the experiment is repeated. Technically speaking, the (initial) seed for the random number generator (in subroutine *comp_rotpert.f*) is computed from the initial date and the number of ensemble members in the SMS script *rot.sms*.

A.1 prepIFS

The sampling is included in prepIFS as an option in the EPS setup. Technically, this causes the variable *EPSSIMPL* to be set to two (see, below). In addition, a new variable *EPSBASIS* is used for specifying the number of SVs (i.e., the dimension of the subspace that is sampled from). Note that this variable *EPSBASIS* does not have any impact on other configurations (i.e., the rotation method) as it is only used if "sampling" has been selected.

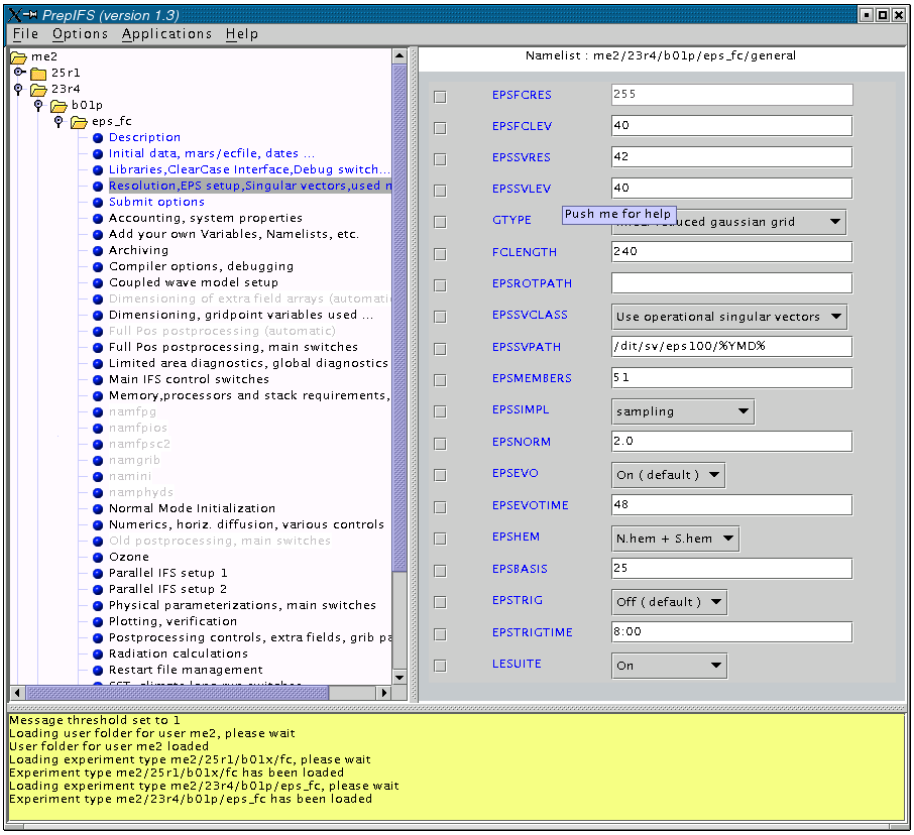

Figure 18: Screenshot of prepIFS window showing EPS setup.

Fig. 18 shows a screenshot of the prepIFS window. This figure reflects the following specifications relevant to the sampling technique (variables *EPSMEMBERS*, *EPSSIMPL*, and *EPSBASIS*):

- $M = 50$ [*EPSMEMBERS* = M + 1 (control)]
- sampling technique (*EPSSIMPL* = "sampling")
- $N = 25$ (*EPSBASIS* = N; number of SVs that is used in the sampling)

A.2 Code

The files *comp_rotmat.f* and *comp_rotpert.f* in directory `src` under the IFS script branch are modified to accommodate for the sampling.

A.2.1 comp_rotmat.f

Additional parameters namely *-y*, *-n*, and *-z* are passed by *rot.sms* to *comp_rotmat* to set up the sampling technique. The option *-y* causes the logical variable *LSAMP* to be set to *TRUE* and trigger the sampling. In addition, the number of SVs that are used for describing the initial–time covariance structure is specified by the parameter *-n $EPSBASIS*. This number is stored in the integer variable *NBASIS* within *comp_rotmat*. The variables *NPERT* and *NSV* are set equal to *NBASIS* to extract the correct number of SVs from the SV input file (e.g., svifs).

A.2.2 comp_rotpert.f

The implementation of the additional command line parameters, as well as the specification of *NPERT*, and *NSV* are done in exactly the same way as in *comp_rotmat* (see above). The scaling that is implied by the rotation matrix (i.e., the diagonal elements of the rotation matrix) is extracted and stored on the variable *beta*. Thereafter the "rotation" matrix is re–allocated with dimensions *NENS* $\times$ *NBASIS* and its columns are filled randomly with realizations of a multinormal distribution. The scaling of the variance level that is implied by the rotation matrix is taken into account through the factor *beta*. This *NENS* $\times$ *NBASIS* matrix is subsequently applied to the set of *NBASIS* SVs to generate the initial time perturbations.

A.3 SMS scripts

Changes are made to the SMS script *rot.sms* in directory `sms` only.

A.3.1 rot.sms

The sampling is triggered by the variable *EPSSIMPL=2*. The number of SVs to use is stored on the variable *EPSBASIS* as specified in prepIFS (see, above). Next, we compute the seeding for the random number generator from the initial date (*BASETIME*) and the number of ensemble members (*EPSNENS*). The new command line options *-y, -n, -z* introduced in *comp_rotmat.f* and *comp_rotpert.f* (see, above) are specified by means of the variable *lnew_opt* and subsequentely passed to the executables.